Cause of the widening of the tropical belt since 1958

Jian Lu[1,2] Clara Deser[1] Thomas Reichler[3]

[1]National Center for Atmospheric Research, Boulder, Colorado, USA

[2]Advanced Study Program/NCAR, Boulder, Colorado, USA

[3]University of Utah, Salt Lake City, UT, USA

Corresponding author:

Jian Lu

George Mason University, Fairfax, Virginia and Center for Ocean-Land-Atmosphere Studies

4041 Powder Mill Road, Suite 302, Calverton, MD 20705-3106

Email: jianlu@cola.iges.org

Abstract

Previous studies have shown that the width of the tropical belt has been increasing since at least the late 1970s based on a variety of metrics. One such metric, the frequency of occurrence of a high-altitude tropopause characteristic of the tropics, is used here to show that the observed widening of the tropics can be accurately replicated by an atmospheric general circulation model forced by the observed evolution of global SST and sea ice distributions as well as the direct radiative effects from both natural and anthropogenic sources. Contrasting this simulation with one forced by the observed SST and sea ice distributions alone reveals that the widening trend can be attributed entirely to direct radiative forcing, in particular those related to greenhouse gases and stratospheric ozone depletion. SST forcing causes no significant change in the width of the tropics, and even a contraction in some seasons.

1. Introduction

There is growing evidence from a variety of data sources that the tropics have been widening, at least since the beginning of the satellite era (1979). For example, Hudson et al. (2007) used the gradient in total ozone between the tropics and subtropics to track an expansion of the tropics in the northern hemisphere by ~1.1º per decade over the period 1979-1991. A similar widening of the tropics was found based on the height of the thermal tropopause from radiosonde data (Seidel and Randel, 2007; Reichler and Held, 2005) and NCEP/NCAR Reanalyses (Reichler and Held, 2005). The tropical expansion is also manifest in terms of tropospheric circulation and hydrology. For example, the distance between the northern and southern hemisphere subtropical jets, a measure of the width of the Hadley Cell, has grown by approximately 2º to 4.5º since 1979 based on satellite-derived tropospheric temperature gradients (Fu et al., 2006); direct estimate of the width of the Hadley cell based on meridional mass streamfunction using wind data from both ERA40 and NCEP/NCAR Reanalyses (Hu and Fu, 2007) yields a widening of the similar order. As a consequence, the subtropical dry zone inferred from satellite measurements of outgoing long-wave radiation (OLR) has also expanded poleward (Hu and Fu, 2007).

Many aspects of the tropical expansion resemble future climate projections from coupled models forced by increasing greenhouse gases (Lu et al., 2007; Seidel et al., 2008), although the observed widening appears to have occurred faster than that simulated by the climate models (Johanson and Fu, 2008). While the observed widening has been speculated to be anthropogenic in origin, no studies (to the best of our knowledge) have

unambiguously identified a precise mechanism. In this study, we make use of two sets of simulations with the GFDL atmospheric model AM2.1 to investigate the origin of the widening of the tropics. In one ensemble simulation, the model is forced by the observed global evolution of SST and sea ice over the 20th century; while in the other ensemble simulation, the estimated radiative forcing from both natural and anthropogenic sources is specified along with the observed SST and sea ice conditions. Our measure of tropical width is based on the thermal tropopause metric of Seidel and Randel (2007), namely the frequency of occurrence of a high-altitude tropopause characteristic of the tropics. Using this definition, we find that only under radiative forcing can the model replicate the observed tropical expansion, and that SST/sea ice boundary forcing produces a contraction of the tropics. By design, the radiative forcing includes both natural and anthropogenic components and does not allow direct attribution of the trend to anthropogenic causes. Nevertheless, our understanding of the distinctive physical signatures of the different radiative forcing agents enables us to suggest that the anthropogenic component is the dominant cause of the widening. The issue of statistical significance of the widening trend in both annual mean and seasonal mean fields is also addressed.

2. Data and Methods

Two sets of reanalysis data for the period 1958-2000 are used in this study: daily tropopause pressure data from NCEP/NCAR (Kistler et al., 2001) and daily temperatures from ERA40 (Uppala et al., 2005) from which we compute daily tropopause pressure. There are warnings against using the reanalysis data prior to 1979 (the beginning of

93 assimilation of satellite data into the reanalysis) for the study of multidecadal variability
94 (Randel et al., 2000). Thus, extra caution has to be taken when examining trends since
95 1958. We find that the tropopause probability density function (PDF) metric of Seidel
96 and Randel (2007), which is also used in this study (see below), is much less susceptible
97 to the effects of changes in instrumentation and observing practices than the monthly
98 mean tropopause height. Indeed, using this metric, we do not find any spurious jumps
99 between 1978 and 1979 in any of the derived time series of tropical width.
100
101 Two sets of ensemble simulations are conducted with GFDL's atmospheric model AM2.1
102 (see Delworth et al., 2006 for model description). One set is forced by specifying the
103 observed monthly evolution of SST and sea ice between 1870 and 2000 (referred to as
104 *SST* experiment) and another by the SST/sea ice plus the estimated radiative forcing from
105 both natural (solar and volcanic aerosol) and anthropogenic sources (well-mixed
106 greenhouse gases, tropospheric and stratospheric ozone, and tropospheric aerosols) over
107 the same period (referred to as *SST+RAD*). The radiative forcing is the same as that used
108 for the 20th century coupled model (CM2) simulations for the Fourth Assessment Report
109 of the Intergovernmental Panel on Climate Change (IPCC AR4) at GFDL. It is worth
110 noting that under the same forcing, the fully coupled GFDL CM2.1, which uses AM2.1
111 as its atmospheric component, can accurately replicate the globally and annually
112 averaged lower stratospheric temperature anomalies over 1979-2003 (Ramaswamy et al.,
113 2006). Each ensemble consists of ten members; each member starts from a different
114 initial condition taken from previous AM2.1 simulations. Experiment *SST+RAD*
115 simulates the past climate with the best possible knowledge of the forcing for the

116 atmosphere, and provides the most comparable case to the real world depicted by the
117 reanalysis data. Assuming linearity, the difference between *SST+RAD* and *SST* may be
118 regarded as the direct response to the radiative forcing. Note that the methodology of
119 specifying both the observed SST and radiative forcing in the atmosphere-only model
120 does not "double count" the atmospheric radiative forcing because only the direct effect
121 is specified and the indirect effect is included in the prescribed SST forcing, and the two
122 effects are linearly additive in a similar experiment (Deser and Phillips, 2008).
123
124 The daily tropopause pressure level is computed from the daily temperature data for the
125 ERA40 reanalysis and each individual member of the AM2.1 simulations. According to
126 the World Meteorological Organization [1957] definition, the tropopause level is
127 identified as the lowest pressure level at which the lapse rate decreases to 2ºC/km and the
128 average lapse-rate between this level and all higher levels within 2 km does not exceed
129 2ºC/km, using the algorithm of Reichler et al. [2003]. The NCEP/NCAR tropopause data
130 also follows the WMO definition.
131
132 For each grid point and each year/season, we computed the PDF of daily tropopause
133 pressure by binning the data into 5 hPa bins, from 50 hPa to 350 hPa. Figure 1 shows the
134 climatological zonal mean of the PDFs for ERA40 and the *SST+RAD* simulations based
135 on the period 1958-1999. The agreement between the two is encouraging, with both
136 showing a dense concentration of low (<120 hPa) tropopause pressure values in the
137 tropics and a bimodal distribution near the subtropics (centered at approximately 35º in
138 each hemisphere). Following Seidel and Randel (2007), we associate tropopause

pressures < 120hPa (or equivalently >15km) with tropical conditions and count the number of tropical tropopause days at each latitude. From this, we define the edge of the tropics as the latitude at which the number of tropical tropopause days exceeds 200 days per year. Defined this way, the mean edges of the tropics are located at the equatorward flanks of the subtropical bimodal distribution. These edges are 29.3ºS (28.0ºS) and 30.0ºN (29.2ºN) for ERA40 (AM2.1 *SST+RAD*) as indicated by the vertical dotted lines in Figure 1. The resulting annual time series of the northern and southern edges of the tropics for the period 1958-1999 (1958-2007 for NCEP/NCAR Reanalysis) are shown in Figure 2 (the starting year for our analysis is dictated by the availability of the ERA40 data set). Analogous time series for each season are provided in the Auxiliary materials (Figure S1)

We estimate the linear trend between 1958 and 1999 using standard linear regression analysis. The estimated trends and their 95% confidence intervals for each season and the year as a whole are shown in Figure 3. The significance test for the trend is conducted following the method proposed by Santer et al. (2000). In their proposed Student's *t*-test, the reduction of effective degrees of freedom due to the serial correlation of the regression residuals is considered in both the estimation of the variance of the residuals and indexing of the critical *t* value. An alternative nonparametric estimate of the significance of the trend is provided in the Auxiliary materials (Figure S2). Both tests lead to qualitatively similar conclusions.

3. Results

Figure 2 shows the annual time series of the tropical edges in both hemispheres for ERA40 (black) and NCEP/NCAR (dashed black) Reanalysis and the ensemble mean of *SST* (green) and *SST+RAD* (red) simulations. We stress that no large spurious discontinuity occurs between 1978 and 1979 in this PDF-based measure of tropical width for either Reanalysis. In each hemisphere, the mean latitude of the tropical edge is similar between *SST+RAD* simulation and NCEP/NCAR Reanalysis, and displaced equatorward by approximately 1º latitude relative to the ERA reanalysis. Thus, on average, the total width of the tropics in the NCEP/NCAR reanalysis and the ensemble mean *SST+RAD* simulation is about 2º latitude narrower than in the ERA40. The simulations with *SST+RAD* forcing exhibit a significant trend during 1958-1999 in each hemisphere: 1.1º for the northern and 1.9º for the southern, equivalent to 0.71º per decade for the total width of the tropical belt. This is similar to that estimated from the Reanalyses (0.70º per decade for ERA40 and 0.79º per decade for NCEP/NCAR). In contrast, the simulations forced by SST/sea ice alone tend to produce a significant shrinking of the tropics (see Figure 3). Similar results hold for the seasonal time series (Figure 3; see also Supplementary Figure S1 for the time series for each season). These findings clearly point to the critical role of direct radiative forcing in producing the widening in our measure of tropical width.

Examining the seasonality of the tropical expansion, we find that both Reanalyses products exhibit significant trends in summer and fall in the northern hemisphere and in all seasons in the southern hemisphere (Figure 3). The *SST+RAD* simulation reproduces the observed seasonality reasonably well. Therefore, despite the uncertainties in the

185 reanalyses and in the forcing of the *SST+RAD* simulation, their consensus on the
186 significance of the tropical expansion makes a strong case for its reality. It is evident that
187 the *SST* experiments simulate a narrowing of the tropics in all seasons in both
188 hemispheres, with significant narrowing during winter, spring and autumn in the northern
189 hemisphere and fall in the southern hemisphere.
190
191 To further demonstrate the characteristics of the tropopause trends, using DJF as an
192 example, we plot in Figure 4 the linear trends superimposed on the climatological mean
193 tropopause PDFs for (a) ERA40, (b) *SST+RAD* simulation, (c) *SST* simulation, and (d)
194 the difference between *SST+RAD* and *SST*. One striking feature in both ERA40 and
195 *SST+RAD* is the continuous dipole structure of the trends throughout the tropics and
196 southern hemisphere: Positive (negative) trends exist along the upper (lower) portion of
197 the mean tropical PDFs, indicative of a rising of the mean tropopause in both the tropics
198 and southern hemisphere extratropics (a slight upward trend is also found at high
199 latitudes of the northern hemisphere). Decomposing the trend into SST forced (Figure 4c)
200 and direct radiatively forced (Figure 4d) components, we find that both contribute to the
201 rise of the tropical tropopause, while direct radiative forcing dominates the rise of the
202 extratropical southern hemisphere tropopause. Even though the rise of the tropical
203 tropopause is due to both SST and direct radiative forcing, the expansion of the tropical
204 tropopause is due solely to radiative forcing as can been seen by the occurrence of
205 positive trends at the outer periphery of the mean tropical PDF in Figure 4d.
206

207 **4. Summary and Discussion**

208 Simulations with GFDL's AM2.1 atmospheric general circulation model driven by the
209 our best knowledge of forcings for the 20th century, including the observed SST and sea
210 ice distributions as well as the direct radiative effects from both natural and
211 anthropogenic sources, reproduces qualitatively, and sometimes quantitatively, the
212 observed widening of the tropics during 1958-1999 as estimated from the ERA40 and
213 NCEP/NCAR Reanalysis data. This result confirms the findings of Seidel and Randel
214 (2007) and corroborates the reality of the expansion of the tropical belt since 1958. By
215 contrasting the results from two sets of experiments, one forced by SST/sea ice alone and
216 the other by SST/sea ice plus direct radiative effects, we demonstrate that our measure of
217 tropical expansion is entirely attributable to direct radiative forcing; SST forcing alone
218 causes no significant change in the width of the tropics, and even a contraction in some
219 seasons. We speculate that the SST-forced contraction might result from the dominance
220 of the upward swing of the Pacific decadal oscillation (PDO) around 1976-77 (Deser et
221 al., 2004; Zhang et al., 1997) and/or the multidecadal variation in Atlantic SSTs
222 (Delworth and Mann, 2000), for the SST pattern of the positive phase of the PDO
223 resembles that of El Nino, which is associated with a contraction of the tropics (Lu et al.,
224 2008).
225
226 Further examination of the temperature response in the model simulations (not shown)
227 reveals that the trends in tropopause pressure and the consequent widening of the tropics
228 is largely a result of stratospheric cooling, a feature consistent with the radiative effects
229 of increased GHGs and stratospheric ozone depletion and in alignment with the notion
230 that the tropopause rise over the past decades was mainly associated with stratospheric

231 cooling but less strongly with tropospheric warming (Seidel and Randel, 2006; Austin
232 and Reichler, 2008).
233
234 In addition to well-mixed greenhouse gases and ozone, the *SST+RAD* experiment also
235 includes variations in solar radiation, and direct scattering effects of anthropogenic and
236 volcanic aerosols. Solar forcing has been shown to warm both the troposphere and
237 stratosphere and should thus exert a rather weak impact on tropopause height. Both types
238 of aerosols were shown to contribute to a downward trend in tropopause heights by
239 warming the lower stratosphere (Santer et al., 2003). Further, we find from Figure 2 that
240 the tropics tend to contract after major volcanic eruptions, thus providing no explanation
241 for the widening. Taken together, the most likely culprits for the widening of the tropics
242 since 1958 are increasing GHGs and stratospheric ozone depletion, both of which are of
243 anthropogenic origin. Identification of their separate roles would require additional
244 experiments with each radiative forcing agent considered individually.
245
246 Finally, we underline that our results are based on the PDF of the tropopause to
247 distinguish between tropics and extratropics. This is only one specific definition of
248 tropical width, and its connection to other approaches, for example those based on
249 tropospheric circulation or hydrological features, remains to be established. Preliminary
250 analysis indicates that the connections between the different measures are complex and
251 hence warrant further investigation.
252
253

Acknowledgements

The authors thank David Schneider for reading the manuscript as NCAR internal reviewer. We are indebted to Tom Delworth and Fanrong Zhang for designing and conducting the AM2.1 model experiments. JL is supported by the UCAR/NCAR Advanced Study Program. The National Center for Atmospheric Research is sponsored by the National Science Foundation. TR is in part supported by NSF Grant ATM 0532280.

References:

Austin, J. and T. Reichler (2008), Long-term evolution of the cold point tropical tropopause: simulation results and attribution analysis. *J. Geophys. Res.*, (in press, online at: http://www.inscc.utah.edu/~reichler/publications/papers/Austin_Reichler_2008_JGR.pdf).

Deser, C., and A. S. Phillips (2008), Atmospheric circulation trends, 1950-2000: the relative roles of sea surface temperature forcing and direct atmospheric radiative forcing. *J. Climate,* doi: 10.1175/2008JCLI2453.1

Deser, C., A. S. Phillips, and J. W. Hurrell (2004), Pacific Interdecadal Climate Variability: Linkages between the Tropics and North Pacific during boreal winter since 1900. *J. Climate,* **17**, 3109-3124.

Delworth, T. L., and M. E. Mann (2000), Observed and simulated multidecadal variability in the Northern Hemisphere. *Clim. Dyn.* **16**, 661–676.

Delworth T. L. and coauthors (2006), GFDL's CM2 global coupled climate models. Part I: Formulation and simulation characteristics. *J. Climate*, **19,** 643-674.

277 Fu, Q., C. M. Johanson, J. M. Wallace and T. Reichler (2006), Enhanced mid-latitude
278 tropospheric warming in satellite measurements. *Science,* **312**, 1179.
279 Hu, Y. and Q. Fu (2007), Observed poleward expansion of the Hadley circulation since
280 1979. *Atmos. Chem. Phys.,* **7**, 5229-5236.
281 Hudson, R. D., M. F. Andrade, M. B. Follette and A. D. Frolov (2007), The total ozone
282 field separated into meteorological regimes-Part II: Northern Hemisphere mid-latitude
283 total ozone trends. *Atmos. Chem. Phys.,* **6**, 5183-5191.
284 IPCC (2007), *Fourth Assessment Report of the Intergovernmental Panel on Climate*
285 *Change* [Solomon, S., D. Qin, M. Manning, Z. Chen, M. Marquis, K.B. Averyt, M.
286 Tignor and H.L. Miller (eds.)]. Chapter 9: Understanding and Attributing Climate
287 Change*,* G. C. Hegerl and F. W. Zwiers et al., Cambridge University Press, Cambridge,
288 United Kingdom and New York, NY, USA, 996 pp.
289 Johanson, C. M., and Q. Fu (2008), Hadley cell widening: model simulations versus
290 observations, *J. Climate*, doi: 10.1175/2008JCLI2620.1
291 Kistler, R. et al. (2001) The NCEP/NCAR 50-year reanalysis: Monthly means CD-ROM
292 and documentation, *Bull. Am. Meteorol. Soc.,* **82**, 247-267.
293 Lu, J., G. A. Vecchi, and T. Reichler (2007), Expansion of the Hadley cell under global
294 warming. *Geophys. Res. Lett.,* **34**, L06805, doi:10.1029/2006GL028443.
295 Lu, J., and G. Chen, and D. Frierson (2008), Response of the zonal mean atmospheric
296 circulation to El Nino versus global warming. *J. Climate*, 21, 5835-5851.
297 Ramaswamy, V., M. D. Schwarzkoph, W. J. Randel, B. D. Santer, B. J. Soden, and G. L.
298 Stenchikov (2006), Anthropogenic and natural influence in the evolution of lower
299 stratospheric cooling. *Science*, **311**, 1138-1141.

Randel, W. J., F. Wu, and D. J. Gaffen (2000), Interannual variability of the tropical tropopause derived from radiosonde data and NCEP reanalyses. *J. Geophys. Res.,* **105**, 15,509-15,524.

Reichler, T. J. and I. M. Held (2005), Evidence for a widening of the Hadley cell. *AMS Conference on Climate Variability and Change*, 2005.

Santer, B. D., T. M. L. Wigley, J. S. Boyle, D. J. Gaffen, J. J. Hnilo, D. Nychka, D. E. Santer, B.D., et al. (2003), Contributions of anthropogenic and natural forcing to recent tropopause height changes. *Science*, **301**, 479–483.

Seidel, D. J., Q. Fu, W. J. Randel, and T. J. Reichler (2008), Widening of the tropical belt in a changing climate. *Nature Geoscience*, **1,** 21-24.

Seidel, D. J. and W. J. Randel (2006), Variability and trends in the global tropopause estimated from radiosonde data. *J. Geophys. Res.,* **111**, D21101, doi:10.1029/2006JD007363.

Seidel, D. J. and W. J. Randel (2007), Recent widening of the tropical belt: Evidence from tropopause observations. *J. Geophys. Res.,* **112**, D20113, doi:10.1029/2007JD008861.

Uppala, S. M., et al. (2005), The ERA40 reanalysis. *Q. J. R. Meteorol. Soc.,* **131**, 2961-3012.

Zhang, Y., J. M. Wallace, and D. S. Battisti (1997), ENSO-like interdecadal variability: 1900–93. *J. Climate,* **10,** 1004–1020.

Figure Captions

Figure 1 Climatological mean (1958-1999), zonally averaged annual PDF (unit is d/year) of tropopause pressure on 5-hPa bins between 75 and 350 hPa for (a) ERA40 and (b) 10 ensemble (*SST+RAD*) simulations. The two vertical lines in each panel demarcate the mean latitude of the tropical edges, which are 29.3ºS and 30.0ºN for ERA40 and 28.0ºS and 29.2ºN for the simulations.

Figure 2 Annual time series of the location of the tropical edges, defined as the latitudes where days with tropopause pressures < 120 hPa (heights > 15 km) exceed 200 days per year. Estimates are from ERA40 (black) and NCEP/NCAR (dashed black) reanalysis data, and from the *SST* (green) and *SST+RAD* (red) simulations. The years of major volcanic eruptions are also indicated.

Figure 3 Linear trend (1958-1999) in the latitude of the tropical edge for the (top) northern and (bottom) southern hemisphere and their corresponding 95% confidence intervals (error bars). Results are based on ERA40 (solid black) and NCEP/NCAR (dashed black) reanalysis data, and on the *SST* (green) and *SST+RAD* (red) simulations.

Figure 4 Linear trend (1958-1999) (shading) (in d/year/decade) and climatological mean (contours) of the daily tropopause pressure PDFs for DJF. Results are for (a) ERA40 reanalysis; (b) *SST+RAD*; (c) *SST*; and (d) (b)-(c). The two vertical lines indicate the mean latitudes of the tropical edges (33.4ºS and 30.2ºN for ERA40; 32.0ºS and 29.5ºN for the simulations).

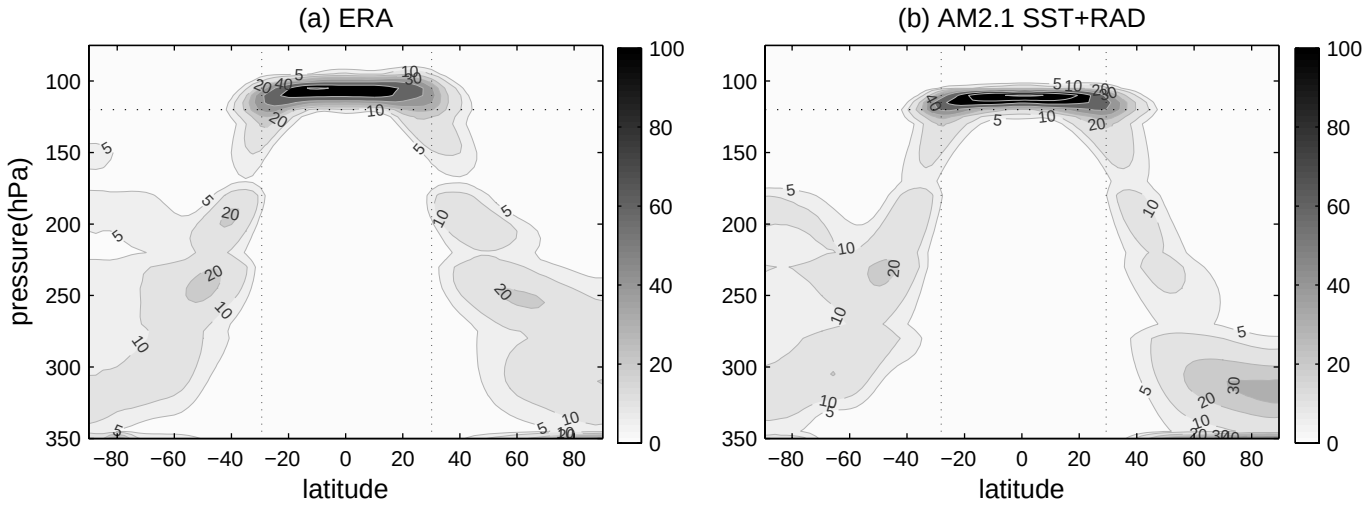
(a) ERA
(b) AM2.1 SST+RAD
pressure(hPa)
latitude
latitude
100
150
200
250
300
350
−80
−60
−40
−20
0
20
40
60
80
0
20
40
60
80
100

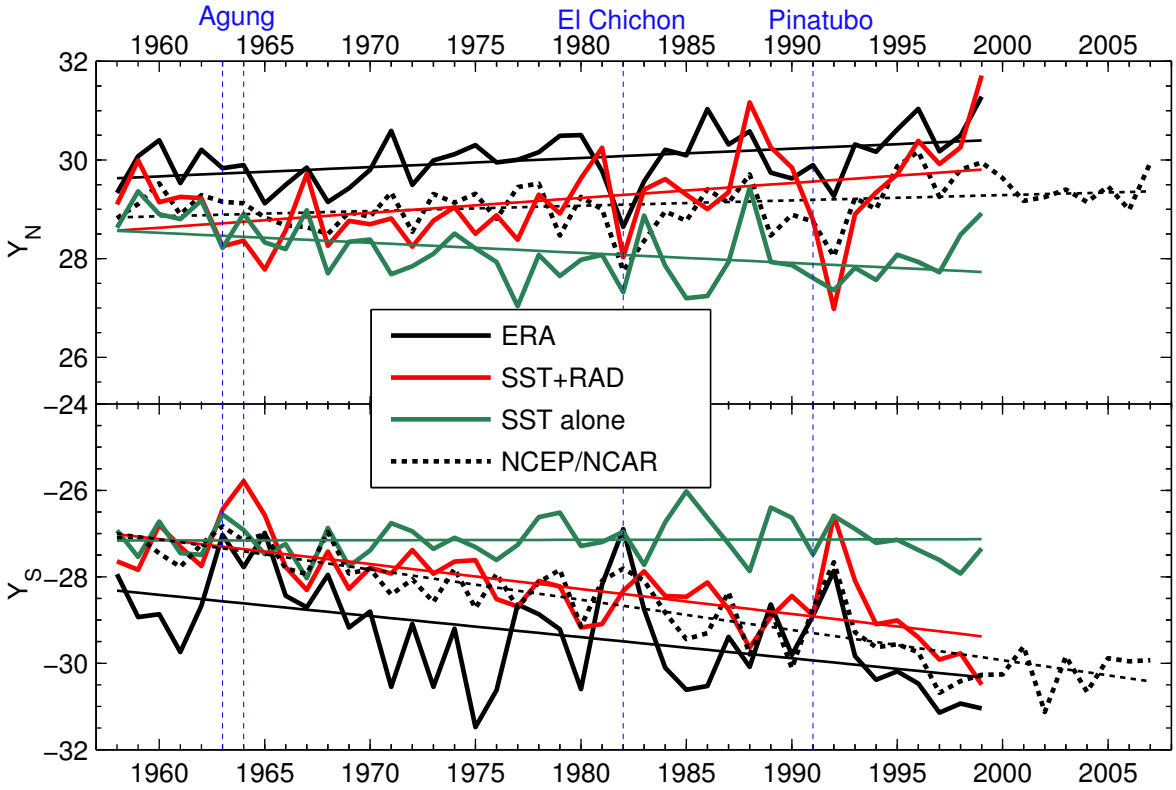
Agung
El Chichon
Pinatubo
1960
1965
1970
1975
1980
1985
1990
1995
2000
2005
32
30
28
26
−24
−26
−28
−30
−32
Y_N
Y_S
ERA
SST+RAD
SST alone
NCEP/NCAR

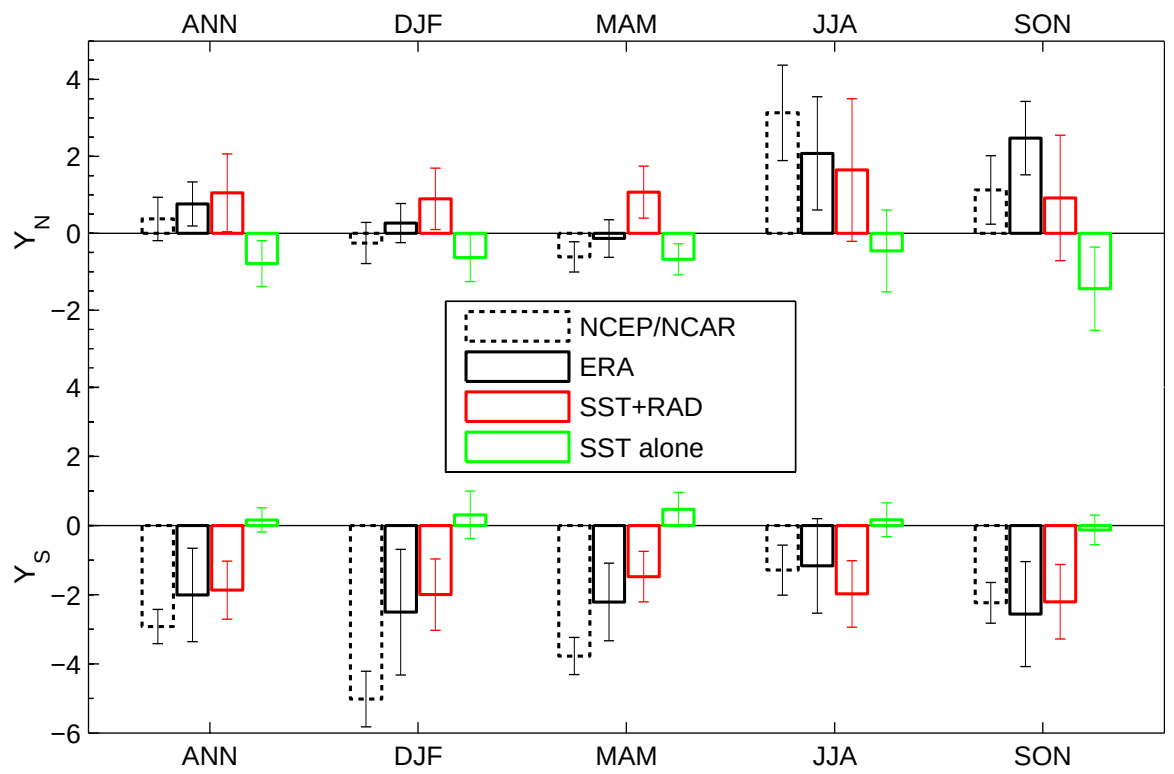
ANN
DJF
MAM
JJA
SON
Y_N
Y_S
4
2
0
−2
4
2
0
−2
−4
−6
NCEP/NCAR
ERA
SST+RAD
SST alone
ANN
DJF
MAM
JJA
SON

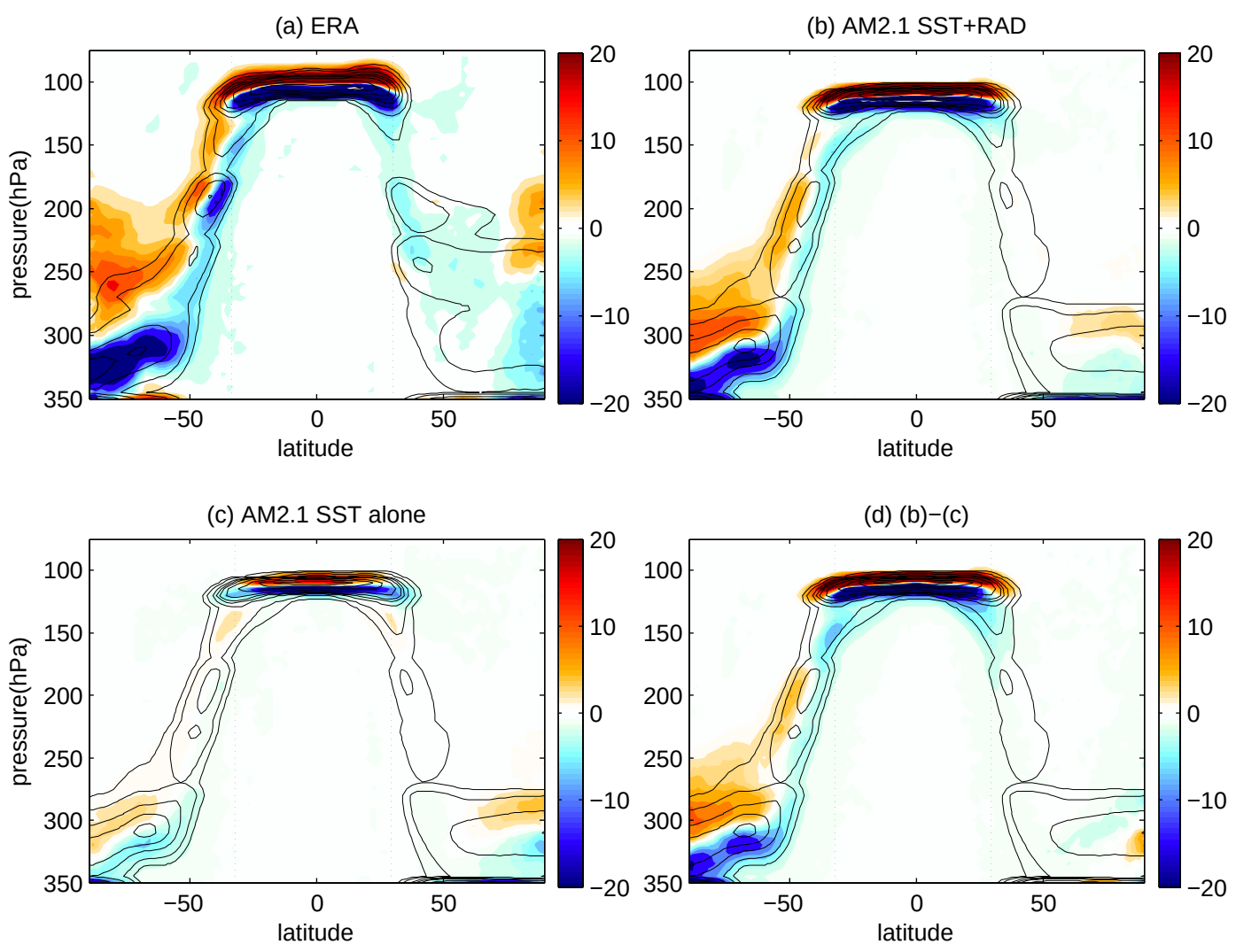
(a) ERA
(b) AM2.1 SST+RAD
(c) AM2.1 SST alone
(d) (b)−(c)
pressure(hPa)
100
150
200
250
300
350
−50
0
50
latitude
20
10
0
−10
−20